Surface Morphology of Homogeneous and Asymmetric Membranes Made from Poly(phenylene oxide) by Tapping Mode Atomic Force Microscope

K. C. KHULBE,* B. KRUCZEK, G. CHOWDHURY, S. GAGNÉ, and T. MATSUURA

Chemical Engineering Department, University of Ottawa, Ottawa, Canada

SYNOPSIS

Surface morphology of asymmetric and homogeneous membranes prepared from poly(phenylene oxide) (PPO) was studied by tapping mode atomic force microscopy (TM AFM). As expected, a significant difference in the morphology between the top and the bottom surfaces of the asymmetric membrane was observed. The images of the top surface revealed a small variation in the vertical direction (6.7 nm), compared to the mean diameter of nodules (62 nm), while the images of the bottom surface were very porous (microfiltration structure). On the other hand, the observed difference in morphology between the top and the bottom surfaces of the membrane prepared by the complete evaporation of the solvent (homogeneous membrane) was rather unexpected. The nodules on the bottom surface were twice as large as those on the top surface. These studies also revealed some differences in the morphology of the top surface of asymmetric and homogeneous membranes. Both surfaces were made up of nodules having a similar size (62–64 nm); however, roughness parameters calculated for the top surface of the asymmetric membrane were approximately two times greater than those for the top surface of the homogeneous membrane. © 1996 John Wiley & Sons, Inc.

INTRODUCTION

The atomic force microscopy (AFM) is a newly developed high-resolution technique to study the morphology of the surfaces of thin films. In the study of membranes, it has been adequately used for the study of the morphology of the biological membranes.[1-7] However, few articles have appeared in the literature for the study of the morphology of synthetic membranes by AFM.[8-13] Fritzsche et al.[8] studied the surface structure and topography of commercially available poly(vinylidene fluoride) microfiltration membranes by AFM. They noticed by the AFM technique uniform nodule aggregates with intermediate-sized pores in their interstitial regions. The nodule aggregates combine to form supernodular aggregates whose boundaries can also be delineated by AFM. Larger pores existed in these boundary regions. Dietz et al.[13] studied the images of the surface of various commercial microfiltration (MF) and ultrafiltration (UF) membranes prepared from polycarbonate, polysulfone, and poly(ether sulfone) by AFM operating in air. They reported pore sizes of UF membranes to be 7.2 and 36.6 nm and pore densities ranging from 88 to 482 pores/μm^2, which values were much higher than those for MF membranes. The porosity was less than 7% for both MF and UF membranes. They suggested that image analysis of the AFM picture can provide detailed information on the pore structure and allows one to determine the most important pore characteristics. No such work has been reported for membranes used for gas separation where pores are very small in comparison with UF or MF membranes.

In the present article, we report the surface morphology of the gas-separation membranes prepared from poly(phenylene oxide) (PPO). It was observed by tapping mode atomic force microscopy (TM AFM) that the top surfaces of both studied membranes were significantly smoother than were the

* To whom correspondence should be addressed.

Journal of Applied Polymer Science, Vol. 59, 1151–1158 (1996)
 CCC 0021-8995/96/071151-08

bottom surfaces, especially in the case of the asymmetric membrane. However, some differences in the morphology between the top surfaces of the asymmetric and homogeneous membranes also were detected.

EXPERIMENTAL

Preparation of Membranes

Both homogeneous and asymmetric membranes were made from PPO (molecular weight = 40,000) using chloroform as a solvent. The solution of PPO (20 wt %) in chloroform was mixed thoroughly and filtered through a 3 μm filter. The membrane was cast from the polymer solution using a casting box to limit the dust. The solution was poured on a glass plate and spread in one continuous smooth motion with a brass casting bar. The thickness of the solution film was 125 μm. The asymmetric membrane was prepared by a wet-phase inversion process. The glass plate containing the solution film was immediately immersed in a gelation bath consisting of methanol for 1 h and then dried in air at room temperature. The homogeneous membrane was prepared by removing the solvent by evaporation at room temperature. To remove the last traces of solvent from the membranes, both membranes were further dried in a vacuum oven (at least 15 Torr) at room temperature for 3 days. The last traces of residual solvent (chloroform) content in each sample was at the zero level as it could not be detected by the mass spectrograph, Model No. VG 7070E (Vacuum Generator, England).

Microscopic Observations

Four small squares of approximately 0.5 cm^2 area (two for the investigation of the top and two for the investigation of the bottom surfaces) were cut from each prepared membrane and glued on metal disks. The images of the surfaces were obtained using TM AFM on a Nanoscope III equipped with a 1553D scanner from Digital Instruments, Santa Barbara, CA.[14] Tapping mode is a new technique developed by Digital Instruments for operating the AFM. The lateral resolution in TM AFM compares favorably to the contact and noncontact AFM; also, the force applied to the sample in TM AFM is significantly lower than that in the contact AFM. Before imaging membrane surfaces, the calibration of the microscope was examined. The distances in the X and Y directions measured on 1 μm gold calibration grating differed less than 2%, while the distance in the Z direction measured on a 180 nm step height calibration standard differed less than 10% from the values provided by the manufacturer.

The membrane surfaces were imaged in three different scan sizes: large (18.1 × 18.1 μm), intermediate (3.54 × 3.54 μm), and small (0.693 × 0.693 μm). The large scan size corresponded to the maximum scan area obtainable with the scanner. It should be emphasized that images of membrane surfaces could be obtained in any scan size equal to or less than the maximum scan size; however, a characteristic morphology of the membrane surface can be revealed only in a particular range of scan sizes, which depends on the size and the distribution of characteristic features of the surface.

Characterization of Membrane Surfaces

Surfaces of membranes were compared in terms of some of the roughness parameters, such as the mean roughness (R_a), the root mean square of the Z data (R_q), and the mean difference in height between the five highest peaks and the five lowest valleys (R_z), as well as in terms of the diameter of the nodules. The comparison was based on the representative images of each of the studied surfaces. The roughness parameters depend on the curvature and size of the TM AFM tip, as well as on the treatment of the captured surface data (planefitting, flattening, filtering, etc.). Therefore, the roughness parameters should not be considered as absolute roughness values.

The mean roughness is the mean value of surface relative to the center plane, the plane for which the volume enclosed by the image above and below this plane are equal, and is calculated as[15]

$$R_a = \frac{1}{L_x L_y} \int_0^{L_y} \int_0^{L_y} |f(x, y)| \, dxdy$$

where $f(x, y)$ is the surface relative to the center plane and L_x and L_y are the dimensions of the surface.

The root mean square of the Z values (R_q) is the standard deviation of the Z values within the given area and is calculated as

$$R_q = \sqrt{\frac{\sum (Z_i - Z_{avg})^2}{N}}$$

where Z_{avg} is the average of the Z values within the given area; Z_i, the current Z value; and N, the number of points within a given area.

The average difference in height between the five highest peaks and the five lowest valleys is calculated relative to the mean plane, which is a plane about which the image data has a minimum variance.

The size of nodules was estimated from cross-sectional profiles of the data along the reference line. An example of the measurement of the diameter of nodules is shown in Figure 1. For each pair of cursers, the horizontal and vertical distances as well as the angle between the cursers are given in the right window. The reported size (diameter) of the nodules is based on the average of at least 50 measurements.

Membrane Testing

Membranes were tested in the constant pressure gas-testing system using pure CO_2 and CH_4 gases. The upstream pressure was 100 psig, while the downstream was at atmospheric pressure. The tests were performed at room temperature. The permeation area was about 10 cm^2.

RESULTS AND DISCUSSION

Asymmetric Membrane

Figures 2 and 3 show the representative 3-D images of the bottom and top surfaces of the asymmetric membrane, respectively. It should be emphasized that the Z axis is expanded relative to the XY plane; therefore, the surfaces are not as "bumpy" as they appear on the images. The surfaces are shown in different scan sizes because of dramatic differences in the morphology between them.

Quantitatively, the differences in the morphology can be expressed in terms of various roughness parameters such as the mean roughness (R_a), the root mean square of vertical data (R_q), and the mean difference between the five highest peaks and the five lowest valleys (R_z). These parameters were calculated for all studied surfaces and the results are summarized in Table I. It can be noticed that the roughness parameters for the bottom surface of the asymmetric membrane are two orders of magnitude greater than for the top surface (Table I).

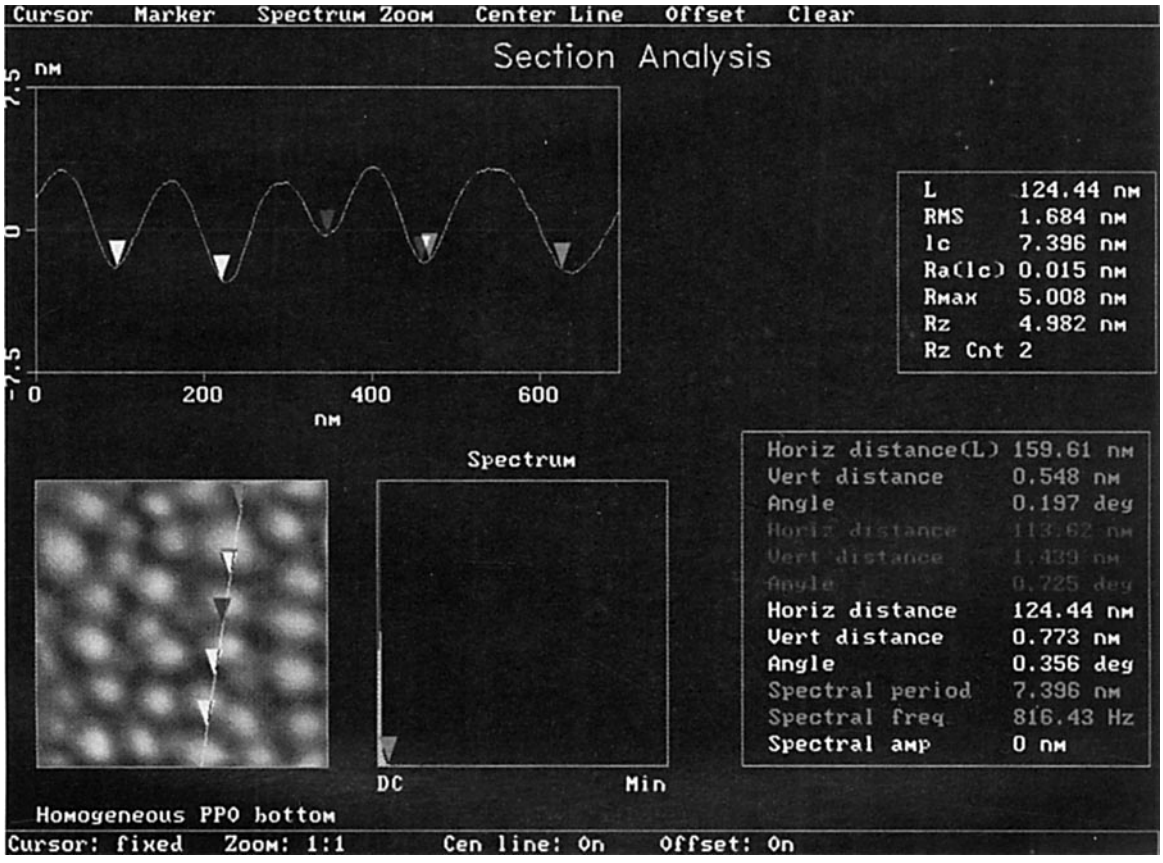

Figure 1 Section analysis of the TM AFM image; a vertical displacement profile of the bottom surface of the homogeneous membrane.

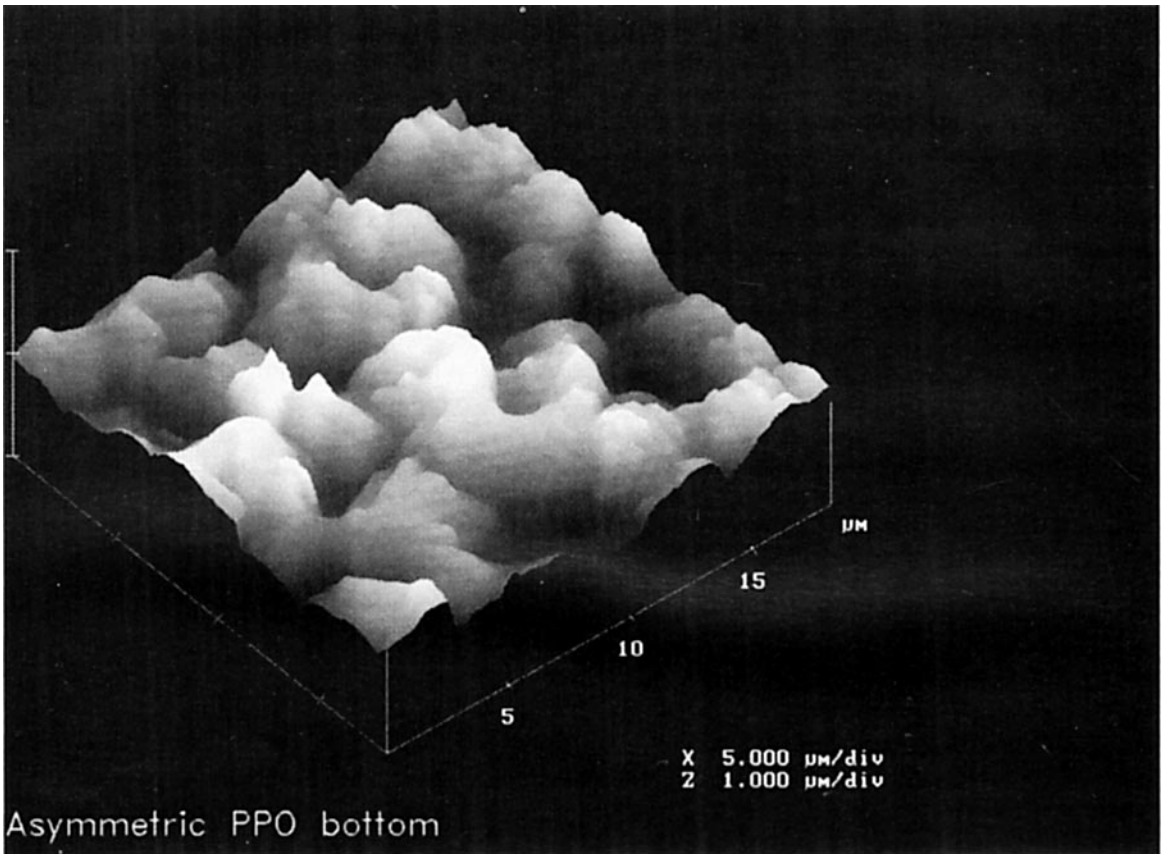

Figure 2 Surface plot of the image by TM AFM of the asymmetric membrane's bottom surface.

Figure 2 reveals the presence of deep depression regions of an area ranging from 2 to 8 μm^2 on the bottom surface of the asymmetric membrane. These depressions are surrounded by high elevation chains having a width up to 5 μm. Referring to the four tiers of structure in integrally skinned membranes proposed by Kesting,[15] the high elevation regions in Figure 2 correspond to supernodular aggregates. It can also be noticed from Figure 2 that the supernodular aggregates are made of spherical grains having a diameter up to several hundred nanometers. These spherical grains can be referred as nodule aggregates.[15]

Figure 3 reveals a nodular structure of the top layer of the asymmetric membrane with the average nodule diameter being approximately 62 nm, which is significantly greater than the size range for nodules stated by Kamide and Manabe[16] and Kesting.[15] The comparison of the variation in vertical direction of the image, R_z = 6.7 nm, with the mean diameter of nodules (d = 62.3 nm), indicates that the top surface is relatively flat. Kesting[15] attributed the flattening of the top surface of integrally skinned asymmetric membranes to the surface tension and the restraining effect of contiguous nodule aggregates. The mechanism of the skin-layer formation of the membrane by dry/wet phase inversion was described recently by Pinnau and Koros.[17] A relatively flat top surface of this membrane may indicate that the interstitial regions are not free of matter but rather that they are the regions of lower polymer density as suggested by Kesting.[15] It could be imagined that polymer chains present in the interstitial regions are distributed more randomly compared to polymer chains present in nodules; however, they could effectively block pores resulting from the packing of spherical or hemispherical nodules. Therefore, it is possible that the macromolecule disposition within the nodule is a determining factor in gas separation as indicated by Kesting.[18] If this was not a case, a membrane with large nodules on the top layer would not be selective for gases.

Based on the permeation tests of the asymmetric membranes, the mean permeability of the membrane for CO_2 was determined to be 5.0×10^{-10} mol/(m^2 s Pa), while the average ideal selectivity for CO_2/

CH_4 was determined to be 35. Therefore, the analysis of 3-D TM AFM images of the top surface of the asymmetric membrane combined with performance tests confirmed that interstitial regions should be considered as regions of lower polymer density which, in combination with nodules, provide a selective layer for gas separation.

Homogeneous Membrane

Figures 4 and 5 show the representative 3-D images of the bottom and top surfaces of the homogeneous membrane, respectively. It can be noticed that both surfaces show a relatively uniform nodular structure; however, nodules on the bottom surface (d_{avg} = 137.5 nm) are twice as large as those on the top surface (d_{avg} = 63.8 nm). A summary of the measurements of the diameters of nodules for both the asymmetric and homogeneous membranes is presented in Table II.

The observed difference in the morphology between the top and bottom surfaces of the homogeneous membrane was rather surprising. In fact, this result questions the appropriateness of the term homogeneous membrane used for the membrane having different morphologies on the top and bottom surfaces. Perhaps it would be more appropriate to refer to this membrane as a dense membrane. On the other hand, the term homogeneous membrane has been widely used for membranes prepared by complete evaporation of the solvent. To avoid confusion, we will continue to use the term homogeneous membrane throughout this article.

Table I Roughness Parameters for Surfaces

Membrane	Surface	R_a (nm)	R_q (nm)	R_z (nm)
Homogeneous	Top	0.376	0.523	3.733
	Bottom	0.757	0.937	4.764
Asymmetric	Top	0.755	0.986	6.749
	Bottom	115.6	835.5	641.1

R_a is the mean roughness; R_q, the root mean square (RMS) of Z values; and R_z, the mean difference between the five highest peaks and the five lowest valleys.

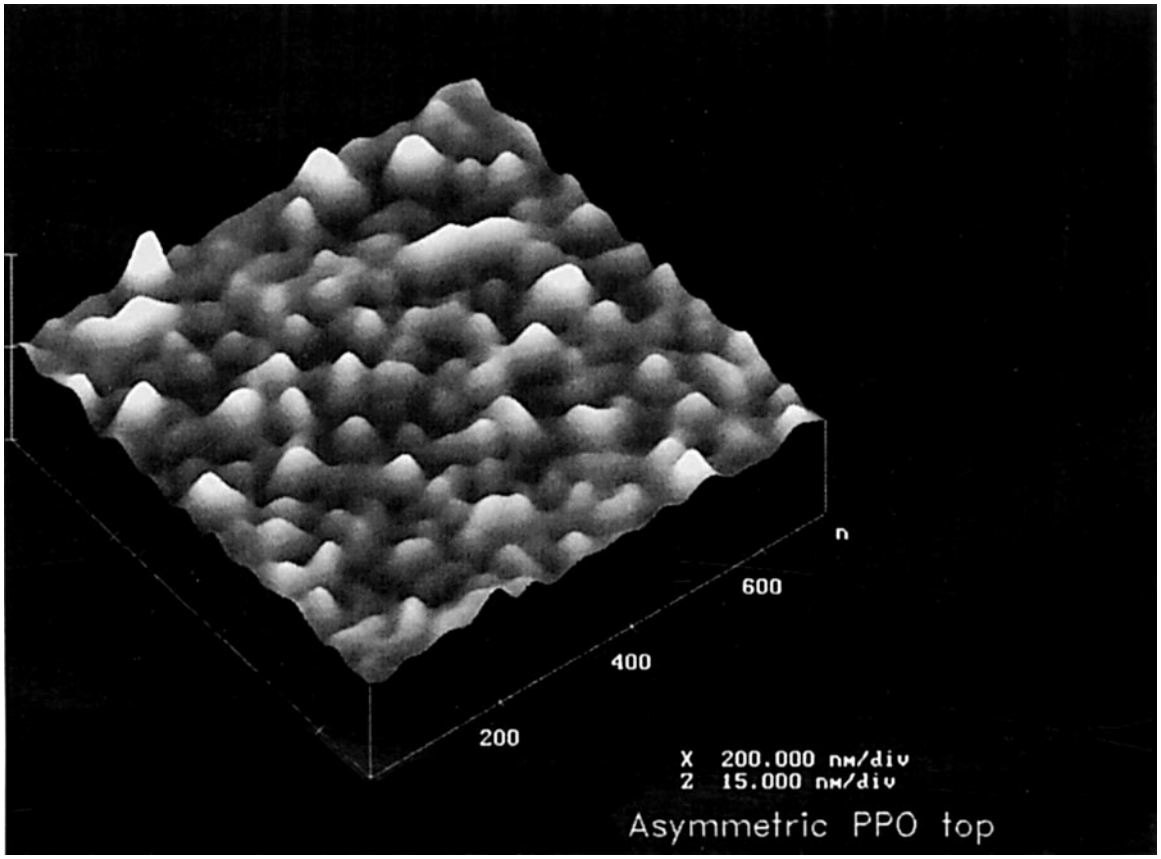

Figure 3 Surface plot of the image by TM AFM of the asymmetric membrane's top surface.

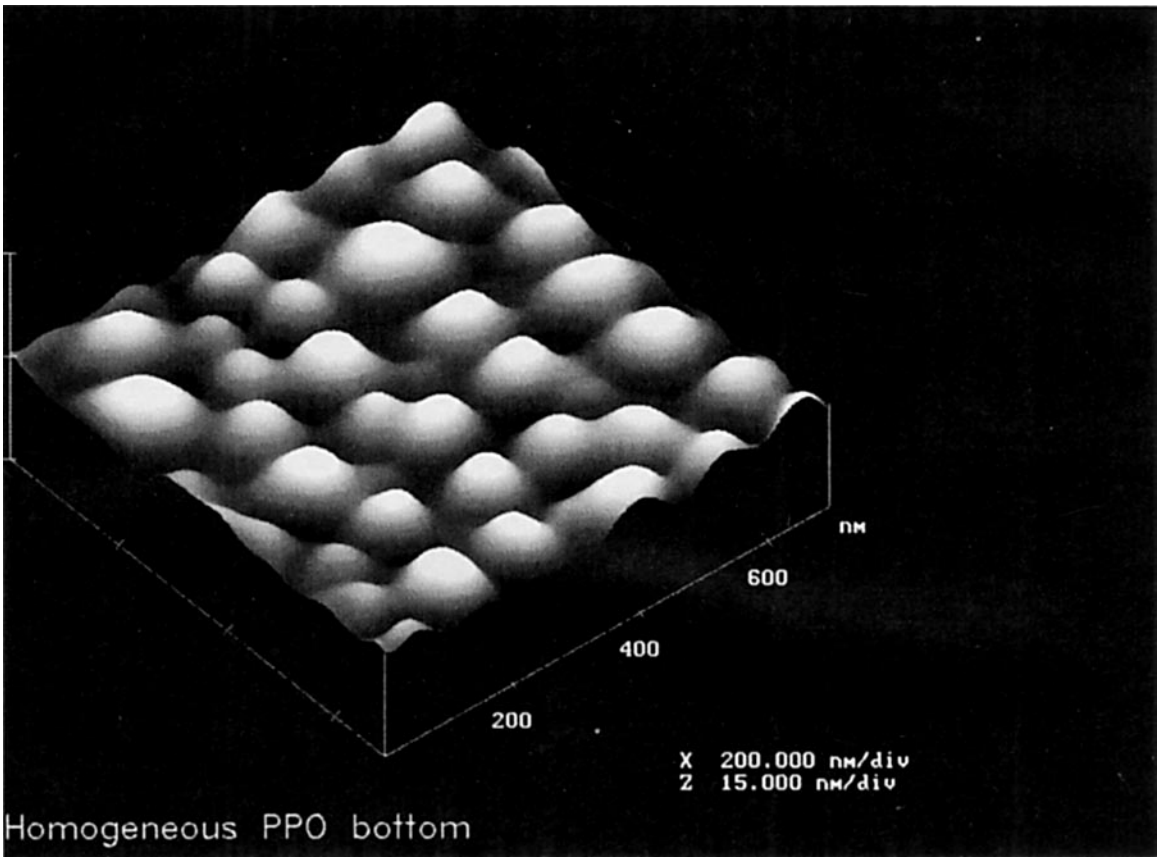

Figure 4 Surface plot of the image by TM AFM of the homogeneous membrane's bottom surface.

The difference in the diameter of nodules on the top and bottom surfaces of the homogeneous membrane could be caused by a different rate of solvent evaporation across the membrane, i.e., the evaporation rate of solvent at the top surface was faster than on the bottom surface. The difference in the evaporation rates increases with the volatility of the solvent and an increase in the initial polymer concentration.

The comparison of the top surfaces of the asymmetric and homogeneous membranes (Figs. 3 and 5, respectively) indicates that the nodules on both surfaces have approximately the same diameters (62–64 nm). Despite this, the top surface of the asymmetric membrane is twice as rough as is the top surface of the homogeneous membrane (Table II). A higher roughness of the asymmetric membrane can be attributed to the quenching of the membrane in methanol during the gelation process.

The performance tests on the homogeneous membrane could not be done. The homogeneous membrane was brittle, and as a consequence, it ruptured in the testing cell after applying 100 psig upstream pressure.

CONCLUSIONS

From the present study, the following conclusions can be drawn for PPO membranes prepared from chloroform:

1. In the case of the asymmetric membrane, the morphology of the top surface is dramatically different from the morphology of the bottom surface. This difference is quantitatively expressed by 2 orders of magnitude greater roughness parameters for the bottom surface compared to the top surface.
2. Except the bottom surface of the asymmetric membrane, all other surfaces are relatively flat, which is indicated by a small variation in the vertical direction compared to the horizontal size of the nodules.

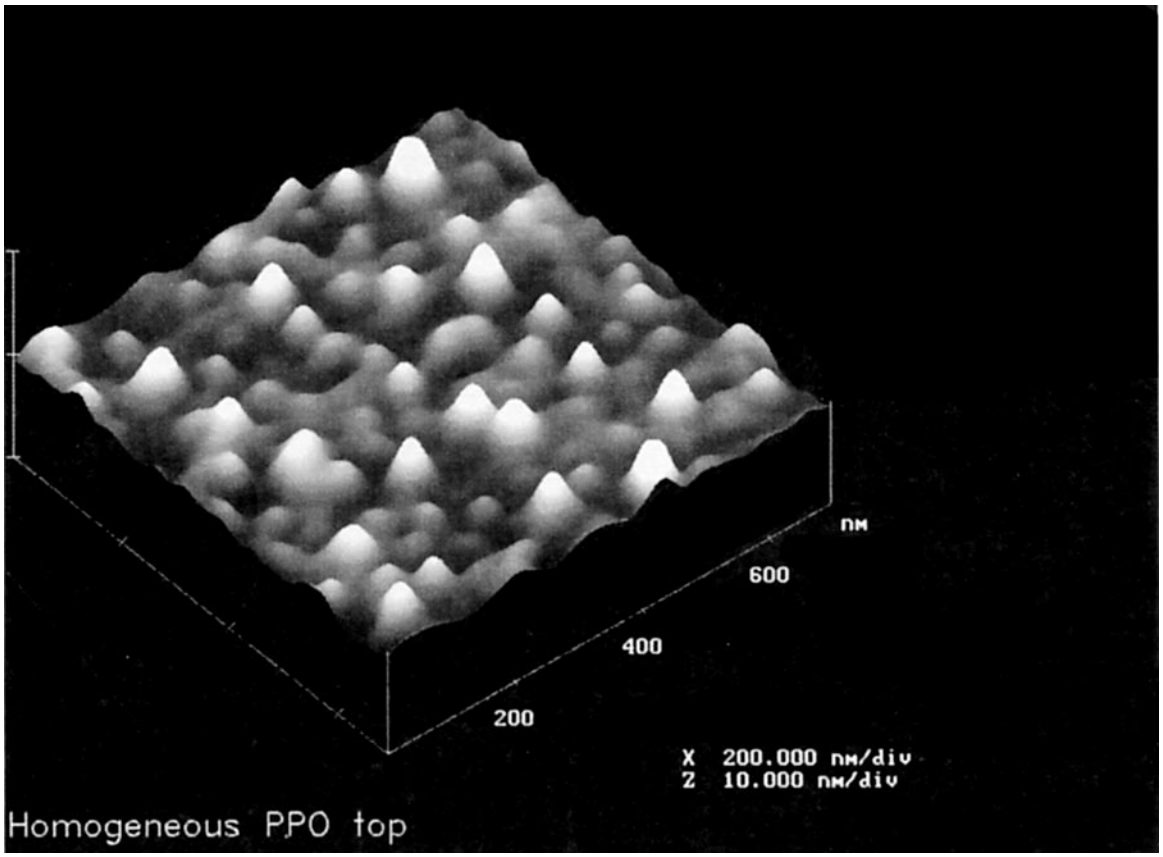

Figure 5 Surface plot of the image by TM AFM of the homogeneous membrane's top surface.

3. 3-D analysis of TM AFM images of the asymmetric membrane combined with the performance data for this membrane (ideal selectivity for CO_2/CH_4 equals 35) indicates that interstitial regions should be considered as regions of lower polymer density, which, in combination with the nodules, provide a selective layer for gas separation.
4. The images of the top and bottom surfaces of the homogeneous membrane revealed a uniform nodular structure of both surfaces; however, nodules on the bottom surface are twice as large as are nodules on the top surface. The difference in the nodular diameter could have resulted from different rates of solvent evaporation from these surfaces.
5. The diameters of nodules on the top surface of the asymmetric and homogeneous membranes are similar; however, the roughness parameters for the top surface of the asymmetric membrane are approximately twice as high as those for the top surface of the ho-

Table II Summary of the Measurement of Nodule Diameter

Membrane	Surface	Min (nm)	Max (nm)	Mean (nm)	St. Dev. (%)
Homogeneous	Top	43.28	89.27	63.8	16.8
	Bottom	97.38	178.55	137.5	20.7
Asymmetric	Top	48.69	75.74	62.3	13.0
	Bottom[a]	230.2	478.1	352.1	30.1

[a] Nodule aggregates.

mogeneous membrane. A higher roughness of the asymmetric membrane can be attributed to the quenching of the membrane in methanol during the gelation process.

The authors acknowledge gratefully that the AFM equipment used in this study was purchased by the British (Consumers) Gas/NSERC Industrial Chair Program.

REFERENCES

1. H. G. Hansma, A. L. Weisenhorn, S. A. C. Gould, R. L. Sinsheimer, H. E. Gaub, G. D. Stucky, C. M. Zaremba, and P. K. Hansma, *J. Vac. Sci. Technol.*, **13**(2), 1282 (1991).
2. H. G. Hansma, M. Bezanilla, F. Zenhausem, M. Adrian, and R. L. Sinsheimer, *Nucl. Acids Res.*, **1**(3), 505 (1993).
3. A. L. Weisenhorn, F. J. Schmitt, W. Knoll, and P. K. Hansma, *Ultramicroscopy*, **42–44**, 1125 (1992).
4. F. J. Schmitt, A. L. Weisenhorn, P. K. Hansma, and W. Knoll, *Thin Solid Films*, **210/211**, 666 (1992).
5. K. Kasper, K. H. Herrmann, P. Dietz, P. K. Hansma, O. Inacker, and H. D. Lehmann, *Ultramicroscopy*, **42–44**, 1181 (1992).
6. H. J. Butt, E. K. Wolff, S. A. C. Gould, B. D. Norhern, C. M. Pearson, and P. K. Hansma, *J. Struct. Biol.*, **105**, 54 (1990).
7. H. G. Hansma, and P. K. Hansma, in Advances in *DNA Sequencing Technology*, Proc. Reprint, SPIE, Jan. 21, 1993, Los Angeles, CA, Vol. 1891, p. 66.
8. A. K. Fritzsche, A. R. Arevalo, M. D. Moore, V. B. Elings, K. Kjoller, and C. M. Wu, *J. Membr. Sci.*, **68**, 65 (1992).
9. P. Dietz, P. K. Hansma, K. H. Herrmann, O. Inacker, and H. D. Lehmann, *Ultramicroscopy*, **35**, 155 (1991).
10. A. K. Fritzsche, A. R. Arevalo, M. D. Moore, C. J. Weber, V. B. Elings, K. Kjoller, and C. M. Wu, *J. Appl. Polym. Sci.*, **46**, 167 (1992).
11. A. Bessieres, M. Meireless, P. Almar, V. Sanchez, R. Coratager, and B. Beauvillair, *Recent Prog. Genie Procedes*, **6**, 111 (22, Memb. Prep., Fouling Emerging Process) (1992).
12. A. K. Fritzsche and C. M. Wu, *Euromembrane ESMST Meeting Proceedings*, Paris, 1992.
13. P. Dietz, P. K. Hansma, O. Inacker, H. D. Lehmann, and K. H. Herrmann, *J. Membr. Sci.*, **65**, 101 (1992).
14. Digital Instruments Inc., NanoScope III, Control System Manual, Santa Barbara, CA, Dec. 1993.
15. R. E. Kesting, *J. Appl. Polym. Sci.*, **41**, 2739 (1990).
16. K. Kamide and S. Manabe, in *Materials Science of Synthetic Membranes*, D. Lloyd, Ed., ACS Symp. Series 269, American Chemical Society, Washington, DC, 1985.
17. I. Pinnau and W. J. Koros, *J. Polym. Sci. Part B Polym. Phys.* **31**, 419 (1993).
18. R. E. Kesting, Paper presented at 195 American Chemical Society Meeting, Toronto, June 7, 1988.

Received February 7, 1995
Accepted August 21, 1995